AIAA JOURNAL
Vol. 41, No. 1, January 2003

Generalized Logarithmic Law and Its Consequences

Matthias H. Buschmann*
Technische Universität Dresden, 01062 Dresden, Germany
and
Mohamed Gad-el-Hak†
Virginia Commonwealth University, Richmond, Virginia 23284-3015

There has been considerable controversy during the past few years concerning the validity of the universal logarithmic law that describes the mean velocity profile in the overlap region of a turbulent wall-bounded flow. Alternative Reynolds-number-dependent power laws have been advanced. We propose herein an extension of the classical two-layer approach to higher-order terms involving the Kármán number and the dimensionless wall-normal coordinate. The inner and outer regions of the boundary layer are described using Poincaré expansions, and asymptotic matching is applied in the overlap zone. Because of the specific sequence of gauge functions chosen, the resulting profile depends explicitly on powers of the reciprocal of the Kármán number. The generalized law does not exhibit a pure logarithmic region for large but finite Reynolds numbers. On the other hand, the limiting function of all individual Reynolds-number-dependent profiles described by the generalized law shows a logarithmic behavior. As compared to either the simple log or power law, the proposed generalized law provides a superior fit to existing high-fidelity data.

I. Introduction

THE universal logarithmic law describing the mean velocity profile in the overlap region of a turbulent wall-bounded flow is a cornerstone of fluid mechanics research. However, there is no physical or mathematical reason to exclude, a priori, a Reynolds-number dependence of such profile. In fact, there has been considerable controversy during the past few years concerning the validity of the log law, and alternative Reynolds-number-dependent power laws have been proposed (for background, see Panton[1] and Buschmann and Gad-el-Hak[2,3]). Afzal[4,5] rigorously demonstrated the equivalence of the log and power laws at very high Reynolds numbers. Herein we extend the classical approach of Izakson[6] and Millikan[7] to higher orders and derive a generalized log law that exhibits explicit dependence on Kármán number.

The turbulent wall-bounded flow is traditionally separated into two distinct, albeit overlapping, zones. The inner layer, where viscosity is important, and the proper velocity and length scales are, respectively, the friction velocity u_τ and the viscous length scale (or wall unit) ν/u_τ, where ν is the kinematic viscosity, $u_\tau \equiv \sqrt{(\tau_w/\rho)}$, τ_w is the shear stress at the wall, and ρ is the fluid density. Quantities expressed in terms of the inner variables are usually written with a $+$ superscript. Sufficiently far from the wall in the outer region, inertia is important, and the proper velocity and length scales are, respectively, the velocity defect $(U_o - u)$ and the boundary-layer thickness δ, where U_o is the velocity outside the boundary layer and $u(x, y)$ is the mean streamwise velocity. An overlap region is presumed to exist for distances from wall $\nu/u_\tau \ll y \ll \delta$.

Izakson[6] and Millikan[7] were among the first to introduce an asymptotic matching procedure to derive a mean velocity profile for the overlap region from the two-layer approach. The first-order result they obtained is the well-known universal log law. Several attempts have been made to extend this law to second and third orders. Among them are Tennekes,[8] Bush and Fendell,[9] Afzal and Yajnik,[10] Afzal,[11] Afzal and Bush,[12] and Panton.[13] One of the earliest attempts to show experimentally the Reynolds-number dependence of the parameters of the classical log law was undertaken by Patel and Head[14] for pipe flow. Analyzing a wide range of experimental data of canonical turbulent boundary layers, Buschmann and Gad-el-Hak[15] showed the necessity of higher-order, Reynolds-number-dependent analysis. The classical approach of Izakson[6] and Millikan[7] was extended to second order by Afzal[11] and to third order by Afzal and Bush.[12] Herein we extend these results to arbitrary higher orders and derive a generalized log law with explicit dependence on the Kármán number. We validate our theory with modern data sets that are accurate as well as cover a broad range of Reynolds numbers.

The paper is organized as follows. Following these introductory remarks, dimensional analysis is used to derive the functional dependence of the mean velocity and its gradient on the wall-normal coordinate and the Kármán number. The generalized log law is then derived in Sec. III. Section IV describes the experimental evidence validating the generalized law. Departure from the generalized law in the outer layer of the boundary layer is then described in Sec. V. Finally, concluding remarks are given in Sec. VI.

II. Mean Velocity Profile

We begin with rudimentary dimensional analysis. Assume a canonical turbulent boundary layer that is free of the effects of three-dimensionality, compressibility, pressure gradient, curvature, roughness, freestream turbulence, etc. The mean velocity profile of such a boundary layer and its gradient are determined by five parameters: fluid density ρ, kinematic viscosity ν, distance from the wall y, an outer length scale δ, and the wall shear stress τ_w. Thus,

$$u = f_1(\rho, \nu, y, \delta, \tau_w), \qquad \frac{\partial u}{\partial y} = f_2(\rho, \nu, y, \delta, \tau_w) \tag{1}$$

In a problem where the primary dimensions are mass, length, and time, the three parameters ρ, ν, and y are independent and cannot be represented by the other two parameters. The remaining parameters τ_w and δ are dependent parameters. According to Buckingham Pi theorem of dimensional analysis, the number of similarity numbers that are needed to describe the problem follows from the difference between the number of all parameters (five) and the number of independent parameters (three). For the canonical turbulent boundary layer, therefore, two similarity numbers Π_1 and Π_2 are needed:

$$\frac{u}{u_\tau} = \Phi_1(\Pi_1, \Pi_2), \qquad \frac{\nu}{u_\tau^2}\frac{\partial u}{\partial y} = \Phi_2(\Pi_1, \Pi_2) \tag{2}$$

$$\Pi_1 = \frac{\nu}{u_\tau y}, \qquad \Pi_2 = \frac{\delta}{y}, \qquad u_\tau = \sqrt{\frac{\tau_w}{\rho}} \tag{3}$$

Received 23 February 2002; revision received 6 August 2002; accepted for publication 6 August 2002.

*Research Associate, Institut für Strömungsmechanik.
†Caudill Eminent Professor and Chair, Department of Mechanical Engineering. Associate Fellow AIAA.

The reciprocal of Π_1 is the local Reynolds number (or distance from the wall expressed in wall units y^+). The quotient Π_2/Π_1 represents the ratio of the characteristic outer length scale and viscous length scale:

$$\Pi_2/\Pi_1 = u_\tau \delta/\nu = \delta^+ \tag{4}$$

The similarity variable δ^+ is called Kármán number. Introducing this result into Eq. (2), we obtain

$$u^+ = \Phi_3(y^+, \delta^+), \qquad \frac{\partial u^+}{\partial y^+} = \Phi_4(y^+, \delta^+) \tag{5}$$

The outer and inner length scales evolve at different rates with Reynolds number, and therefore the Kármán and Reynolds numbers are closely related. To derive that relation, define a Reynolds number based on the momentum thickness and the velocity outside the boundary layer:

$$Re_\theta \equiv U_o \delta_\theta/\nu \tag{6}$$

This Reynolds number characterizes the outer layer and is related to the Kármán number as follows:

$$\delta^+ = \frac{u_\tau}{U_o}\frac{\delta}{\delta_\theta} Re_\theta = \sqrt{\frac{C_f}{2}}\frac{\delta}{\delta_\theta} Re_\theta \tag{7}$$

where C_f is the skin-friction coefficient, which, like all of the other variables in this equation, depends on distance from the leading edge. Using data for the skin friction and mean velocity profiles from different flat-plate experiments, Gad-el-Hak and Bandyopadhyay[16] have shown the following empirical relation to be valid over a wide range of Reynolds numbers:

$$\delta^+ = 1.168(Re_\theta)^{0.875} \tag{8}$$

Thus, the Kármán number grows downstream at a slower rate than does the Reynolds number. On a semi-infinite flat plate the outer and inner length scales are forever disparting, the boundary layer never achieves true self-preservation, and the Reynolds-number effects on all statistical turbulence quantities persist indefinitely.[16]

III. Generalized Log Law

At sufficiently high Kármán number the influence of the outer coherent structures (which scale with δ) diminishes on the inner zone, and the influence of the inner coherent structures (which scale with ν/u_τ) diminishes on the outer zone. The interaction between the two zones decreases as well, but never goes away completely. At any finite, albeit high, Reynolds number, viscosity and inertia both maintain a small influence on the overlap region between the inner and outer zones.

An asymptotic expansion for the inner layer of the discussed canonical boundary layer can now be written as a Poincaré series:

$$u^+ \sim u_1^+(y^+) + u_2^+(y^+)\gamma_2(\delta^+) + u_3^+(y^+)\gamma_3(\delta^+) + \cdots \tag{9}$$

Here u^+ and y^+ denote, respectively, the nondimensional velocity u/u_τ and wall-normal coordinate yu_τ/ν. For the outer layer the corresponding expansion reads

$$U \sim U_1(\eta) + U_2(\eta)\Gamma_2(\delta^+) + U_3(\eta)\Gamma_3(\delta^+) + \cdots \tag{10}$$

with $\eta = y/\delta$ and $U = (U_o - u)/u_\tau$. The dependence of the velocity profiles on δ^+ is separated into gauge functions γ_i and Γ_i, which are functions only of δ^+, but not necessarily identical functions.

Referring to Poincaré expansions similar to those just shown, Panton[13] states that "while the first term in an expansion is reasonably well defined, subsequent terms can differ depending on the sequence of gauge functions chosen and on the scaling parameters employed in the nondimensional variables." Splitting the mean velocity profile into two expansions causes a loss of boundary condition for both. To compensate, a matching condition for Eqs. (9) and (10) is introduced. Originally, Millikan[7] restricted the matching condition to the first-order normalized gradient, which is physically a matching of mean spanwise vorticity. This restriction is not necessary, however, at least from a mathematical point of view. The next order is a matching of the vorticity flux. In general, it has to be demanded that all normalized derivatives of the inner and outer series expansions are in agreement. Therefore, the first-order ($y^+ \to \infty$, $\eta \to 0$, and $\delta^+ \to \infty$) matching condition for arbitrary order of the gradient reads

$$y^{+^k}\frac{\partial^k u^+}{\partial y^{+^k}} \approx \eta^k \frac{\partial^k U}{\partial \eta^k}, \qquad k = 1, 2, 3, \ldots \tag{11}$$

Here k denotes the order of the derivative, not to be confused with the order of approximation. To fulfill the general matching condition, a certain sequence of gauge functions has to be chosen. Because turbulence is not a closed problem mathematically, the selection of this sequence of gauge functions always involves some additional assumptions, preferably physically based ones. Based on a consideration of the governing equations of the mean motion of fully developed pipe and channel flows, Afzal[11] introduced the following gauge functions for a second-order analysis:

$$\gamma_2 = \Gamma_2 = \epsilon = 1/\delta^+ \tag{12}$$

This type of gauge function can be generalized as $\epsilon^{(j-1)} = 1/\delta^{+(j-1)}$, where $j = 1, 2, \ldots, n$ is the order of approximation. It can readily be shown that such a sequence of gauge functions satisfies Eq. (11) for all k.

According to the original approach of Millikan,[7] only the terms of lowest order of the Poincaré expansions have to be matched. The price for that procedure is that all higher-order terms exhibiting the Kármán number must be neglected. Introducing Eqs. (9) and (10) into the generalized matching condition (11), we obtain

$$\sum_{j=1}^{n} \epsilon^{j-1} y^{+^k} \frac{\mathrm{d}^k u_j^+}{\mathrm{d}y^{+^k}} + \mathcal{O}(\epsilon^n) \approx \sum_{j=1}^{n} \epsilon^{j-1} \eta^k \frac{\mathrm{d}^k U_j}{\mathrm{d}\eta^k} + \mathcal{O}(\epsilon^n) \tag{13}$$

For $k = 1$ the lowest-order term of Eq. (13) becomes

$$y^+ \frac{\mathrm{d}u_1^+}{\mathrm{d}y^+} + \mathcal{O}(\epsilon) \approx \eta \frac{\mathrm{d}U_1}{\mathrm{d}\eta} + \mathcal{O}(\epsilon) \tag{14}$$

Each side of Eq. (14) is asymptotic to a constant, which leads to

$$y^+ \frac{\mathrm{d}u_1^+}{\mathrm{d}y^+} = A_1 + \mathcal{O}\left(y^{+^{-t}}\right), \qquad \eta \frac{\mathrm{d}U_1}{\mathrm{d}\eta} = A_1 + \mathcal{O}(\eta^s) \tag{15}$$

where $t > 0$ and $s > 0$ (cf. Gill[17]). If the higher-order terms of y^+ and η in Eq. (15) are neglected, the usual matching condition is obtained. Integration then leads to the classical log and defect laws

$$u^+ = A\,\ell n(y^+) + C, \qquad U = A\,\ell n(\eta) + c \tag{16}$$

with the parameters A, C, and c, which are independent of any similarity number. Here A denotes $1/\kappa$, the reciprocal of the Kármán constant (not to be confused with the Kármán number δ^+).

To find the higher-order ϵ terms in Eq. (14), one first has to find the higher order y^+- and η terms in Eq. (15). With respect to the next gauge function γ_2, these terms were introduced as integral powers of $1/y^+$ and η by Afzal.[11] From Eq. (15) then follows

$$u_1^+ = A_1\,\ell n(y^+) + C_1 + \sum_{i=1}^{m} \frac{E_{1,i}}{y^{+^i}}$$

$$U_1 = A_1\,\ell n(\eta) + c_1 + \sum_{i=1}^{m} e_{1,i}\eta^i \tag{17}$$

Introducing Eq. (17) into Eq. (14) and collecting terms of order ϵ, the next matching condition is found:

$$y^+ \frac{\mathrm{d}u_2^+}{\mathrm{d}y^+} - e_{1,1}y^+ + \mathcal{O}(\epsilon^2) \approx \eta \frac{\mathrm{d}U_2}{\mathrm{d}\eta} + \frac{E_{1,1}}{\eta} + \mathcal{O}(\epsilon^2) \tag{18}$$

Because of the similar mathematical structure of the first matching condition (14) and the second (18), it can be assumed that each

side of Eq. (18) is again asymptotic to a constant. Integrating and introducing the higher order y^+ and η terms then leads to the next-order term of the mean velocity profile

$$u_2^+ = A_2 \ln(y^+) + C_2 + e_{1,1} y^+ + \sum_{i=1}^{m} \frac{E_{2,i}}{y^{+i}}$$

$$U_2 = A_2 \ln(\eta) + c_2 + \frac{E_{1,1}}{\eta} + \sum_{i=1}^{m} e_{2,i} \eta^i \tag{19}$$

Repeating this procedure leads to the generalized inner law, valid to order $\epsilon^{(n-1)}$,

$$u^+ = A_1 \ln(y^+) + C_1 + \sum_{i=1}^{m} \frac{E_{1,i}}{y^{+i}} + \sum_{j=2}^{n} \epsilon^{j-1} \left[A_j \ln(y^+) + C_j + \sum_{i=1}^{j-1} B_{j,i} y^{+i} + \sum_{i=1}^{m} \frac{E_{j,i}}{y^{+i}} \right] \tag{20}$$

and the generalized defect law

$$U = A_1 \ln(\eta) + c_1 + \sum_{i=1}^{m} e_{1,i} \eta^i + \sum_{j=2}^{n} \epsilon^{j-1} \left[A_j \ln(\eta) + c_j + \sum_{i=1}^{j-1} \frac{b_{j,i}}{\eta^i} + \sum_{i=1}^{m} e_{j,i} \eta^i \right] \tag{21}$$

Here $A_j, C_j, c_j, B_{j,i}, b_{j,i}, E_{j,i}$, and $e_{j,i}$ denote constants that can only be determined from experiments. Differentiating and rearranging Eqs. (20) and (21) leads to the left-hand side

$$y^+ \frac{\mathrm{d}u^+}{\mathrm{d}y^+} = A_1 - \frac{E_{1,1}}{y^+} - \frac{E_{1,2}}{y^{+2}} - \frac{E_{1,3}}{y^{+3}} - \cdots + A_2 + B_{2,1}\eta - \epsilon \frac{E_{2,1}}{y^+} - \epsilon \frac{E_{2,2}}{y^{+2}} - \cdots + A_3 + \epsilon B_{3,1}\eta + B_{3,2}\eta^2 - \epsilon^2 \frac{E_{3,1}}{y^+} - \epsilon^2 \frac{E_{3,2}}{y^{+2}} - \cdots \tag{22}$$

and the right-hand side

$$\eta \frac{\mathrm{d}U}{\mathrm{d}\eta} = A_1 + e_{1,1}\eta + e_{1,2}\eta^2 + e_{1,3}\eta^3 + \cdots + A_2 - \frac{b_{2,1}}{y^+} + \epsilon e_{2,1}\eta + \epsilon e_{2,2}\eta^2 + \cdots + A_3 - \epsilon \frac{b_{3,1}}{y^+} - \frac{b_{3,2}}{y^{+2}} + \epsilon^2 e_{3,1}\eta + \epsilon^2 e_{3,2}\eta^2 + \cdots \tag{23}$$

of the general matching condition (13) for $k = 1$. From these relations it follows that the matching condition can only be satisfied if the following constraints are true:

$$B_{j,i} = e_{j-i,i}, \qquad E_{j-i,i} = b_{j,i} \tag{24}$$

By means of complete induction, it can be shown that if Eq. (13) is satisfied for $k = 1$ it is also satisfied for all higher-order derivatives.

The preceding analysis indicates that pure log regions, as they are proposed by Millikan,[7] Österlund et al.,[18] Zanoun et al.,[19] and others using the classical approach, are not exhibited by the generalized law proposed here. The nonlogarithmic, higher-order terms of y^+ and δ^+ persist throughout the entire overlap region and for all finite Reynolds numbers. From Eqs. (20) and (21) it is clear that the usual constants of the classical log law (16) are functions depending on the Kármán number. Because of the asymptotic behavior of the generalized law concerning δ^+, this dependence persists also for high Reynolds numbers. It has to be regarded as Reynolds-number effects and clearly distinguished from the low-Reynolds-number effects (cf. Spalart[20]). Although the latter are related to incompletely developed turbulent motion, the Reynolds-number effects discussed here are caused by the persistent influence of friction and inertia forces within the overlap region.

IV. Experimental Evidence of the Generalized Law

The constants in Eqs. (20) and (21) must be determined from experimental data. It is to be expected that the dependence on the Kármán number is weak and diminishes asymptotically as δ^+ increases. Therefore an accurate data set with a wide range of δ^+ is required. Such a data set was created by compiling several modern experimental and numerical data bases from different authors as shown in Table 1. In both numerical and physical experiments the uncertainty in measuring the mean velocity is typically better than $\pm 2\%$, whereas wall shear stress is measured or computed to within $\pm 5\%$. Österlund[21] used oil-film interferometery and reports skin-friction accuracy better than $\pm 4\%$, whereas Osaka et al.[22] used a floating element to measure directly τ and claims an accuracy of ± 1–2%. Roach and Brierley[23] utilized the Clauser's method, the momentum balance approach, and a Preston tube. They report that the values of the skin friction as measured by all three methods agree to within 2%.

As we have done in a companion paper,[3] we explain here the process by which we selected the specific data sets to be analyzed. First, we searched for recently published boundary-layer data covering a broad range of Reynolds numbers, with an eye on the reliability and credibility of both the researchers who generated the data and the archival journals that published the results. Preference was given to experiments in which the wall skin friction was measured or computed independently of any assumption of the law governing the overlap region and to publicly available computerized data sets. Second, we excluded pipe and channel flow data, such as those from the recent superpipe experiments at Princeton University. Unlike zero-pressure-gradient boundary layers, fully developed pipe flows do not continue to evolve downstream and do not possess freestream. Lastly, we felt that five independent data sets were quite adequate to show all of the trends sought. Therefore, many good data sets were not included. A graph with 50 data sets will look needlessly cramped, and our selection decision by no means should be construed as a verdict against any of the excluded data, some of which are considered classical albeit unavailable in the form of computer files.

Table 1 Analyzed sets of velocity profiles (VP) of zero-pressure-gradient turbulent boundary layers

Data set	No. of profiles	Probe	Re_θ range	δ^+ range	Symbol[a]
Österlund[21]	70 VP	SHW[b]	2.53×10^3–27.32×10^3	684–6147	■
Osaka et al.[22]	7 VP	SHW	8.6×10^2–6.04×10^3	355–1988	▲
K. S. Choi (private communication, Sept. 1999, Udine, Italy)	1 VP	SHW	1.14×10^3	492	★
Roach and Brierley[23]	16 VP	SHW	5×10^2–2.7×10^3	183–845	●
Spalart[20]	2 VP	DNS[c]	6.4×10^2–1.41×10^3	325–650	♦

[a]The table provides the key to all symbols used in Figs. 1 and 4.
[b]SHW: single hot-wire probe.
[c]DNS: direct numerical simulations.

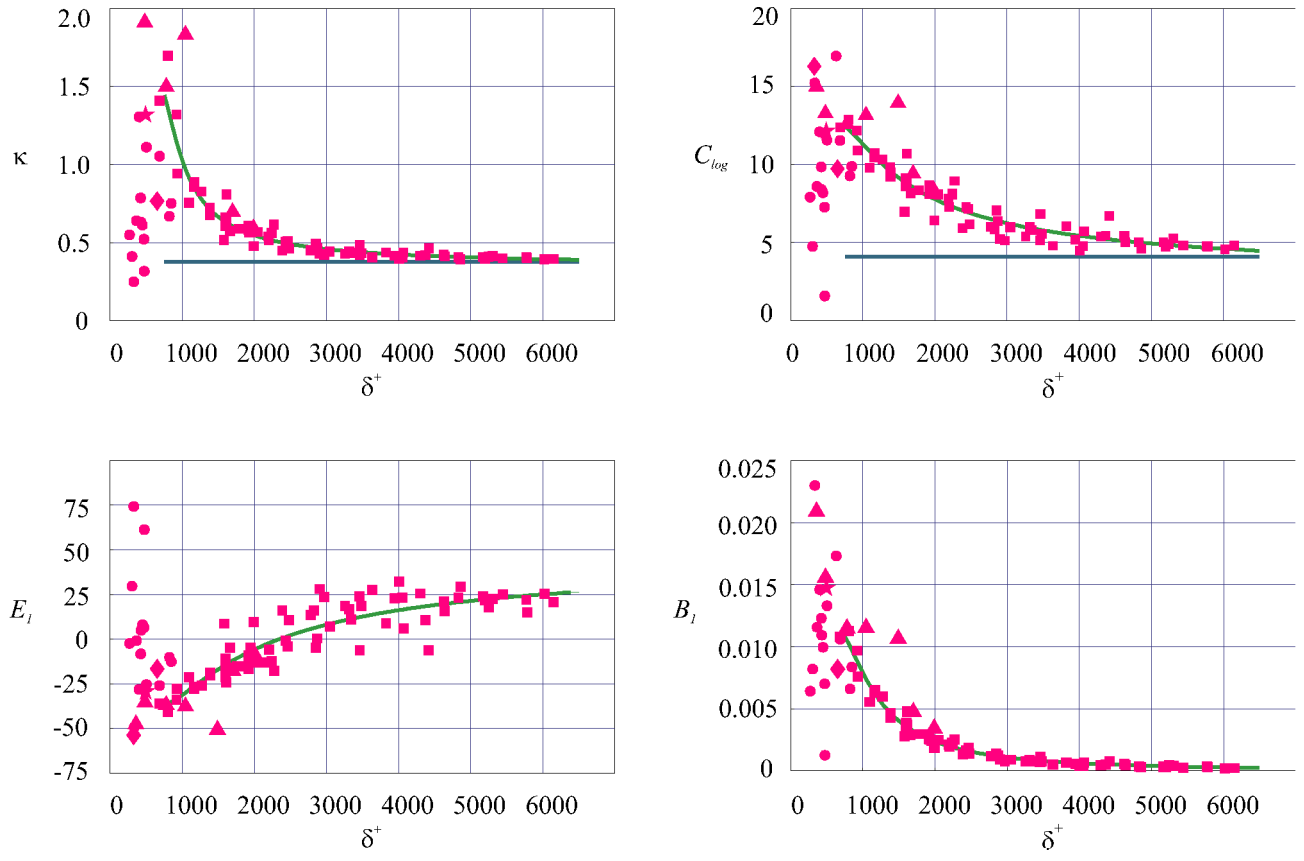

Fig. 1 Parameters of the generalized inner law: blue line, parameters of standard logarithmic law according to Österlund et al.[18]; and green line, regression function of results obtained from Österlund's data. See Table 1 for key to all symbols.

Ignoring y^+ terms of power ± 2 and higher, a simplified version of the generalized inner law (20) results:

$$u^+ = A\,\ell n(y^+) + C_{\log} + E_1/y^+ + B_1 y^+ \tag{25}$$

where

$$A = \sum_{j=1}^{n} \epsilon^{j-1} A_j, \qquad C_{\log} = \sum_{j=1}^{n} \epsilon^{j-1} C_j$$

$$E_1 = \sum_{j=1}^{n} \epsilon^{j-1} E_{j,1}, \qquad B_1 = \sum_{j=2}^{n} \epsilon^{j-1} B_{j,1} \tag{26}$$

denote the parameters of the simplified law. Equation (25) is valid to order $\epsilon^{(n-1)}$. In other words, the Reynolds-number-dependent terms are retained in this equation.

Using the Levenberg–Marquardt algorithm (cf. Gill et al.[24]), a nonlinear fit of the data from Table 1 was carried out to compute the four parameters in Eq. (26), and the results are depicted in Fig. 1. As expected, all parameters asymptote to constant values for infinite Kármán number. They show the predicted dependence on δ^+. For the highest Kármán number achieved in Österlund's data ($\delta^+ = 6{,}147$; $Re_\theta = 27.32 \times 10^3$), κ reaches a value of 0.39, $C_{\log}$ becomes 4.57, and the intercept of the defect law c becomes 3.91. These values are in good agreement with $\kappa = 0.38$, $C_{\log} = 4.1$, $c = 3.6$ computed by Österlund et al.,[18] and $\kappa = 0.39$, $C_{\log} = 4.42$ computed by Perry et al.[25] from the Princeton superpipe data. All other parameters appearing in Eqs. (20) and (21) asymptote to zero for $\delta^+ \to \infty$. For very low Kármán numbers ($\delta^+ \leq 600$) the parameters depicted in Fig. 1 drop or increase sharply. This behavior indicates low-Reynolds-number effects.

Traditionally, semilog plots of u^+ vs y^+ are used to compare the inner law with experimental data. This is only useful if the analyzed mean velocity profiles do not depend on an additional parameter. The inner law (20) is a function of two variables: the nondimensional coordinate y^+ and the Kármán number δ^+. Therefore it is useful to plot the experimental values u^+_{exp} vs the theoretical values $u^+_{\text{theor}}(y^+, \delta^+)$. In case the theoretical mean velocity profiles are in agreement with the experimental data, all points in a linear-linear plot would collapse on a straight line passing by the origin and having a slope of 45 deg. If the theory fails or is not valid in certain regions of the profile, the points depart from the diagonal. This test is done herein using the experimental data base by Österlund[21] (Fig. 2) and Osaka et al.[22] (Fig. 3). To compare to the generalized law, corresponding plots were drawn for the simple log laws proposed by Österlund et al.[18] ($\kappa = 0.38$, $C_{\log} = 4.1$, for $Re_\theta \geq 6 \times 10^3$) and by Osaka et al.[22] ($\kappa = 0.41$, $C_{\log} = 4.9$, for $Re_\theta \geq 2.5 \times 10^3$). Additionally the power law proposed by Barenblatt et al.[26,27]

$$u^+ = C_P y^{+\alpha} \tag{27}$$

was analyzed. This law with Reynolds-number-dependent parameters was originally derived for pipes and later extended to the self-similar intermediate region adjacent to the viscous sublayer of a canonical turbulent boundary layer. The original Reynolds-number-dependent values for the coefficient C_P and the power α, as computed from the Österlund's data by Barenblatt et al.,[27] were used herein. For Osaka et al.'s data the power-law parameters computed by Buschmann and Gad-el-Hak[15] were used.

The left-hand columns of Figs. 2 and 3 show the complete set of velocity profiles from, respectively, Österlund[21] and Osaka et al.[22] over the entire boundary-layer thickness for all three laws. The right-hand column of either figure shows zoomed-in plots of the overlap region. The profiles are colored according to their individual Kármán number like a rainbow from red (lowest δ^+ value) to blue (highest δ^+ value). This coloring scheme allows the observer to spot readily any inherent Reynolds-number dependence.

In both Figs. 2 and 3 the first row depicts the theoretical power law by Barenblatt et al.,[27] the second row depicts the classical log law by Österlund et al.[18] (Fig. 2) or by Osaka et al.[22] (Fig. 3), and the third row depicts the generalized inner law as derived herein.

Although the power law shows more or less an intersecting region of all profiles (Figs. 2a, 2b, 3a, and 3b), for the simple log

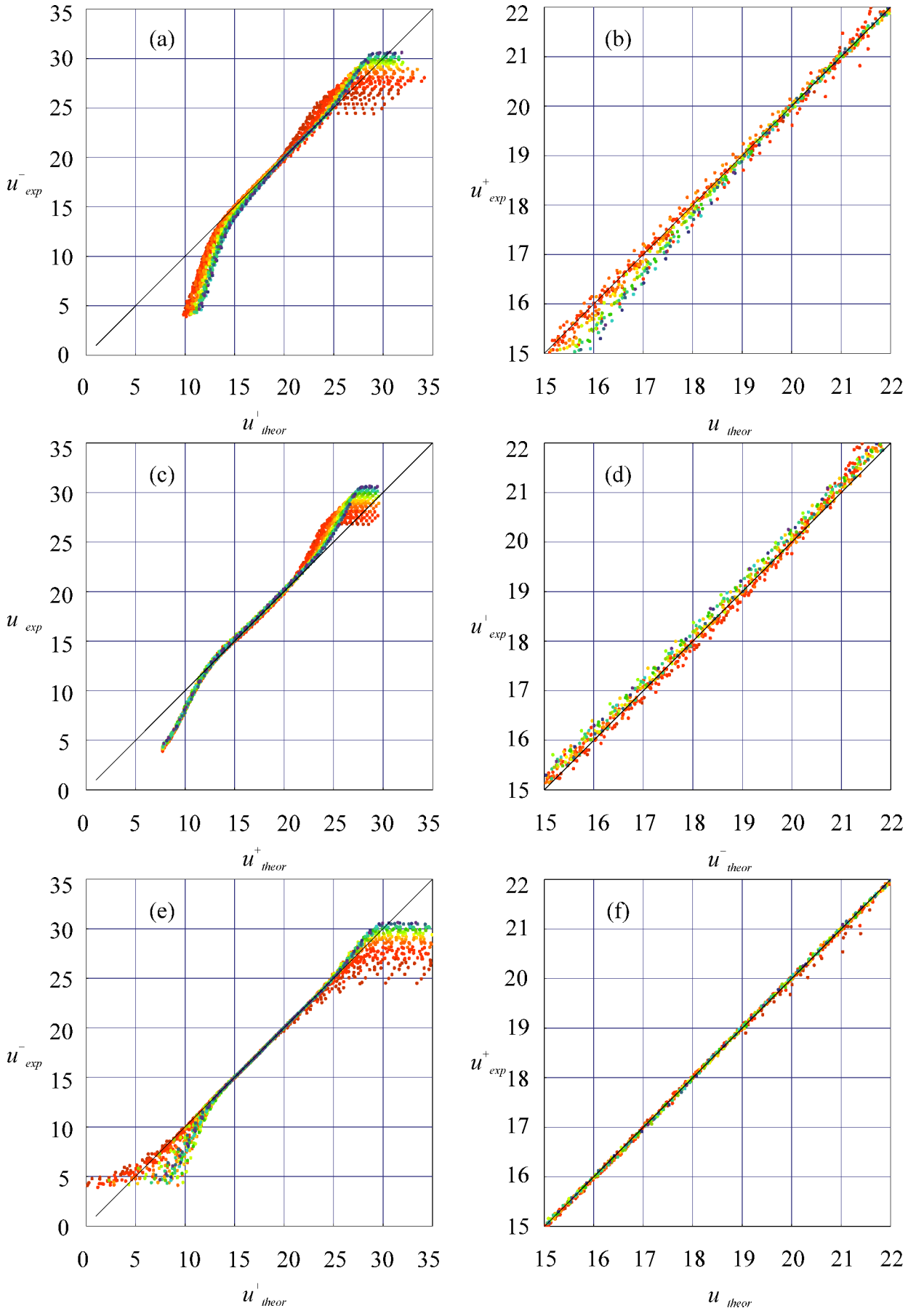

Fig. 2 Comparison of different mean velocity laws with experimental data by Österlund[21]: first row, power law by Barenblatt et al.[27]; second row, classical log law by Österlund et al.[18]; third row, generalized inner law, present work. The right-hand column is a zoomed-in version of the left-hand column, emphasizing the overlap region. The profiles are colored according to their individual Kármán number like a rainbow from red (lowest value) to blue (highest value).

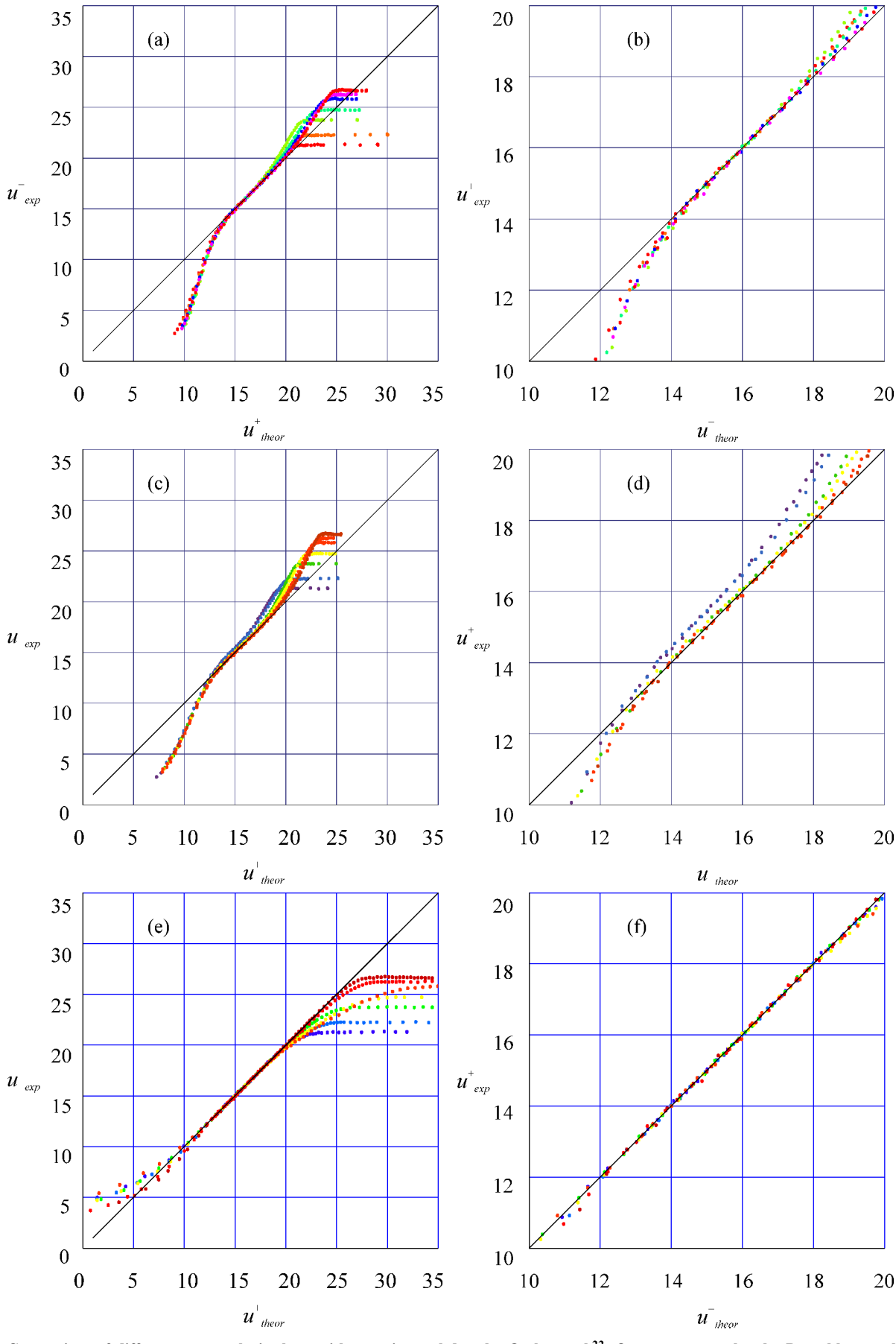

Fig. 3 Comparison of different mean velocity laws with experimental data by Osaka et al.[22]: first row, power law by Barenblatt et al.[27] with parameters according to Buschmann and Gad-el-Hak[15]; second row, classical log law by Osaka et al.[22]; third row, generalized inner law, present work. The right-hand column is a zoomed-in version of the left-hand column, emphasizing the overlap region. The profiles are colored according to their individual Kármán number like a rainbow from red (lowest value) to blue (highest value).

laws by Österlund et al.[18] and Osaka et al.[22] all profiles are grouped in a band around the diagonal (Figs. 2c, 2d, 3c, and 3d). The reasons for the departures are different for both laws. The power law fits the data in an upper region of the overlap zone. However, for the usual log-law region the power law does not exhibit the correct Kármán number dependence. Therefore a rainbow-like distribution of the colors is found for lower values of u^+ (see especially Fig. 2b). The log law with constant parameters is obviously not sufficient for the data to collapse completely with the diagonal. The remaining δ^+ dependence is represented in a rainbow-like distribution of the colors (Figs. 2d and 3d). The slight concave shape of the band denotes the neglected influence of the higher-order terms of y^+. Note that Österlund's log law is valid between $y^+ = 200$ and $\eta = 0.15$, which is equivalent to $u^+ = 18.04$ for the inner border and $u^+ = 18.20$–22.03 for the outer border. The resemblance of Fig. 2c to traditional velocity profiles plotted on a semilog paper is fortuitous. The abscissa here is u^+_{theor}, not $\log y^+$. Finally, applying the generalized inner law (20), with its Reynolds-number-dependent parameters computed from the data, leads to a collapse of all data with the diagonal in an extended overlap zone. Only a very mild random scatter that is caused by the experimental error can be gleaned in the closeup view of the overlap region (Figs. 2f and 3f). As compared to either the simple log or power law, the generalized law clearly provides a superior fit to existing data.

One can argue that the better fit exhibited in Figs. 2f and 3f results from the larger number of free parameters (four) in the generalized log law as compared to the two free constants in the classical log and power laws. To check this point, we plotted several functions, for example, polynomials, with as many degrees of freedom as the generalized log law. None of those plots compared favorably to those in the third row of either Fig. 2 or Fig. 3. In fact, the polynomial plots showed more scatter than that for the simple log and power law. The additional terms in the generalized log law are based on physical arguments, whereas a randomly selected function with as many degrees of freedom is not.

V. Limiting Functions and the Departure Parameters

To represent the entire mean velocity profile of a turbulent boundary layer, Coles[28] combined the inner law and the defect law to give the following empirical relation:

$$u^+(y^+) = f(y^+) + \Delta u^+(\eta) = f(y^+) + \pi w(\eta) \tag{28}$$

where $\Delta u^+(\eta)$ is the strength of the wake component in wall units, π is the wake parameter (maximum deviation from the inner law), and $w(\eta)$ is the universal wake function. Coles[28] found that for canonical turbulent boundary layers π increases up to $Re_\theta \approx 6 \times 10^3$. However, an asymptotic state does not seem to be achieved because above $Re_\theta \approx 15 \times 10^3$; the wake parameter starts to decrease again very slowly.[16]

Coles[28] used a universal function $f(y^+)$ for the law of the wall. Universal in this context means that this function depends only on the wall-normal coordinate y^+. For the inner law (20) discussed here, such a function exists only for $\epsilon \to 0$. Therefore, $f(y^+)$ in Eq. (28) has to be substituted by the limiting function $u_0^+(y^+)$ of the inner law

$$u^+(y^+, \delta^+) = u_0^+(y^+) + \Delta u^+(\eta, \delta^+) \tag{29}$$

The limiting function (or envelope) of the inner law (20) is found by rewriting this law for $\epsilon \to 0$:

$$u_0^+ = A_1 \ln(y^+) + C_1 + \sum_{i=1}^{m} \frac{E_{1,i}}{y^{+i}} \tag{30}$$

For $y^+ \to \infty$ the limiting function $u_0^+(y^+)$ becomes identical with the classical log law (16). Rewriting and rearranging Eq. (29) using Eqs. (20) and (30) leads to the departure function of the generalized inner law

$$\Delta u^+ = \sum_{j=2}^{n} \sum_{i=1}^{j-1} \epsilon^{j-i-1} B_{j,i} \eta^i + \sum_{j=2}^{n} \epsilon^{j-1} \left[A_j \ln(y^+) + C_j + \sum_{i=1}^{m} \frac{E_{j,i}}{y^{+i}} \right] \tag{31}$$

Different from Coles's wake function, this departure function is not built as the deviation of an individual profile in the outer zone from its own overlap region. Instead, the departure function used here is the deviation of an individual profile in the outer zone from the limiting function of the inner law. The two functions become identical only at infinite Reynolds number, but at any finite Reynolds number the two functions cannot be, strictly speaking, directly compared.

Analogous to the limiting function and the departure function of the generalized inner law, a limiting function and a departure function of the generalized outer law are derived as follows:

$$U_0 = A_1 \ln(\eta) + c_1 + \sum_{i=1}^{m} e_{1,i} \eta^i \tag{32}$$

$$\Delta U = \sum_{j=2}^{n} \sum_{i=1}^{j-1} \epsilon^{j-i-1} \frac{b_{j,i}}{y^{+i}} + \sum_{j=2}^{n} \epsilon^{j-1} \left[A_j \ln(\eta) + c_j + \sum_{i=1}^{m} e_{j,i} \eta^i \right] \tag{33}$$

Here the outer departure function is defined as the deviation of an individual outer profile from the corresponding limiting function.

Similar to Coles' wake parameter π, two departure parameters Π_i and Π_o, which denote the maximum departure of an individual profile from the generalized inner or outer limiting function, can be defined as follows:

$$\Delta u^+ = \sum_{j=2}^{n} B_{j,j-1} \eta^{j-1} = \Pi_i \sum_{j=2}^{n} B^*_{j,j-1} \eta^{j-1} \tag{34}$$

$$\Delta U = \sum_{j=2}^{n} \frac{b_{j,j-1}}{y^{+j-1}} = \Pi_o \sum_{j=2}^{n} \frac{b^*_{j,j-1}}{y^{+j-1}} \tag{35}$$

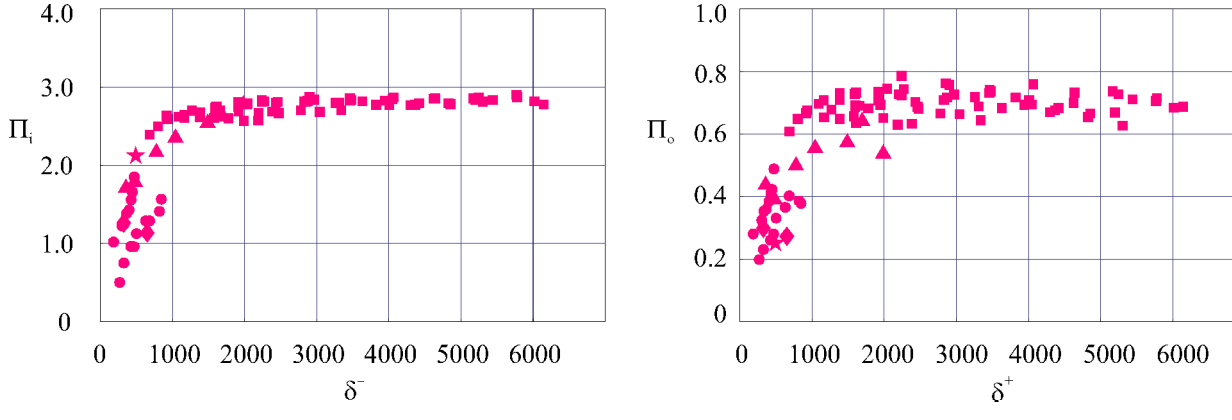

Fig. 4 Departure parameter for the generalized inner law (left) and for the generalized defect law (right). See Table 1 for key to all symbols.

Using the data from Table 1, the inner and outer departure parameters are calculated and compiled in Fig. 4. Above $\delta^+ \approx 2000$ ($Re_\theta \approx 6 \times 10^3$), both parameters show constant values of $\Pi_i = 2.84$ and $\Pi_o = 0.7$. A constant wake parameter π for the classical log law was found for high Reynolds numbers by DeGraaff and Eaton[29] using the log-law constants from Österlund et al.[18] This finding is consistent with the result presented here, as the limiting function of the inner law becomes identical with the classical log law for $y^+ \to \infty$.

VI. Conclusions

The second-order theory that was originally derived by Afzal[11] and the third-order theory developed by Afzal and Bush,[12] for both pipe and channel flows, are extended here to arbitrary higher-order terms. Both the inner and outer generalized laws are successfully applied to the canonical turbulent boundary layer and exhibit explicit dependence on the Kármán number.

The open parameters of the inner and outer generalized laws were obtained from experimental data. It was found that all parameters including the Kármán constant κ and the intercept $C_{\log}$, which are constants in the classical log law, depend asymptotically on the Kármán number. As illustrated in Fig. 1, the difference between the simple log law and the generalized law is quite large at Kármán number of the order of 1000, but quite modest at δ^+ above 6000.

As it contains higher-order y^+ terms, the new generalized law covers a much wider range of wall-normal distances as compared to the simple log or power law. At typical laboratory Reynolds numbers the classical log law covers distances from the wall in the range of $y^+ \approx 50$–300, whereas in the case of the generalized log law the overlap region extends over the range $y^+ \approx 25$–1000, an almost fourfold increase.

As compared to either the simple log or power law, the proposed generalized law provides a superior fit to existing high-fidelity data. The implication of this finding is that the mean velocity profile of a canonical turbulent boundary layer depends on the physical characteristics of the turbulent motion especially on the ratio of outer and inner length scales. If this ratio becomes infinite, the influence of friction disappears, and all of the parameters of the proposed generalized law asymptote to constant values, with some parameters asymptoting to zero.

The classical log law with constant parameters is found to be the limiting function (or envelope) of all individual profiles with finite Kármán and Reynolds numbers. The parameters of this limiting function are in good agreement with the parameters found by Österlund et al.[18] and Perry et al.[25] for high-Reynolds-number flows. It is shown that the maximum departures of experimentally obtained velocity profiles from the limiting functions of the generalized inner and defect laws are constants above $\delta^+ \approx 2000$.

The results presented herein and in the companion paper[3] might help settle the ongoing debate concerning the precise law governing the mean velocity profile of the canonical turbulent boundary layer. Using the method of fractional difference to statistically analyze some of the best mean velocity data presently available, Buschmann and Gad-el-Hak[3] have concluded that such data do not indicate any statistically significant preference toward either the simple log law or the power law, even when the parameters of the latter are allowed to optimally change with Reynolds number. In the present paper the superiority of the generalized log law over both the simple log and power laws has been demonstrated. The effect of the additional terms appearing in the generalized log law diminishes as y^+ and δ^+ increase, making it evident why Österlund et al.[18] advocated a simple, Reynolds-number-independent log law but only above $y^+ \approx 200$ and for Re_θ exceeding 6×10^3, which value increased to 8×10^3 in subsequent papers and presentations dealing with both boundary layers and channel flows (e.g., see Zanoun et al.[19]). It appears more reasonable to admit Reynolds-number effects via the generalized law and thus to be able to describe all wall-bounded flows at all Reynolds numbers above those where turbulence is not quite fully developed, say Re_θ above 2×10^3. This means Re_θ above those at which low-Reynolds-number effects are present. As an additional bonus, our proposed law covers a much wider range of wall-normal distances.

The Reynolds-number effects on the canonical mean velocity profile demonstrated in this paper are modest in absolute terms but can have profound effect on our understanding and treatment of wall-bounded flows in general. Reynolds-number effects on higher-order statistics such as root-mean-square values of the velocity and pressure fluctuations, skewness, spectra, etc., are much stronger as amply illustrated in the review paper by Gad-el-Hak and Bandyopadhyay.[16] Understanding and quantifying all of those effects are essential to our ability to extrapolate low-Reynolds-number laboratory and numerical results to the much higher Reynolds number encountered in typical field applications.

Acknowledgments

The authors thank K. S. Choi, A. J. Chorin, J. Meinert, S. J. Mochizuki, and J. M. Österlund for generously sharing their results and for useful discussion.

References

[1] Panton, R., "Power Law or Log Law; That is NOT the Question," *Bulletin of the American Physical Society*, Vol. 45, No. 9, 2000, p. 160.

[2] Buschmann, M. H., and Gad-el-Hak, M., "The Logarithmic Law in Turbulent Boundary Layers: the Debate Continues," *Proceedings of the Seventh International Congress on Fluid Dynamics and Propulsion* [CD-ROM], edited by A. Serag El Din, Paper CEF-22, Cairo Univ., Cairo, 2001.

[3] Buschmann, M. H., and Gad-el-Hak, M., "Debate Concerning the Mean Velocity Profile of a Turbulent Boundary Layer," *AIAA Journal* (to be published).

[4] Afzal, N., "Power Law and Log Law Velocity Profiles in Fully Developed Turbulent Pipe Flow: Equivalent Relations at Large Reynolds Numbers," *Acta Mechanica*, Vol. 151, Nos. 3 and 4, 2001, pp. 171–183.

[5] Afzal, N., "Power Law and Log Law Velocity Profiles in Fully Developed Turbulent Boundary Layer Flow: Equivalent Relations at Large Reynolds Numbers," *Acta Mechanica*, Vol. 151, Nos. 3 and 4, 2001, pp. 195–216.

[6] Izakson, A., "Formula for the Velocity Distribution near a Wall," *Zhurnal Eksperimental'noi i Teoreticheskoi Fiziki*, Vol. 7, 1937, pp. 919–924.

[7] Millikan, C. B., "A Critical Discussion of Turbulent Flows in Channels and Circular Tubes," *Proceedings of the Fifth International Congress on Applied Mechanics*, edited by J. P. Den Hartog and H. Peters, Wiley, New York, 1939, pp. 386–392.

[8] Tennekes, H., "Outline of a Second-Order Theory of Turbulent Pipe Flow," *AIAA Journal*, Vol. 6, No. 9, 1968, pp. 1735–1740.

[9] Bush, W. B., and Fendell, F. E., "Asymptotic Analysis of Turbulent Channel and Boundary-Layer Flow," *Journal of Fluid Mechanics*, Vol. 56, Pt. 4, 1972, pp. 657–681.

[10] Afzal, N., and Yajnik, K., "Analysis of Turbulent Pipe and Channel Flows at Moderately Large Reynolds Number," *Journal of Fluid Mechanics*, Vol. 61, Pt. 1, 1973, pp. 23–31.

[11] Afzal, N., "Millikan's Argument at Moderately Large Reynolds Number," *Physics of Fluids*, Vol. 19, No. 4, 1976, pp. 600–602.

[12] Afzal, N., and Bush, W. B., "A Three-Layer Asymptotic Analysis of Turbulent Channel Flow," *Proceedings of the Indian Academy of Sciences (Mathematical Sciences)*, Vol. 94, 1985, pp. 135–148.

[13] Panton, R., "Scaling Turbulent Wall Layers," *Journal of Fluid Engineering*, Vol. 112, Dec. 1990, pp. 425–432.

[14] Patel, V. C., and Head, M. R., "Some Observations on Skin Friction and Velocity Profiles in Fully Developed Pipe and Channel Flows," *Journal of Fluid Mechanics*, Vol. 38, Pt. 1, 1969, pp. 181–201.

[15] Buschmann, M. H., and Gad-el-Hak, M., "Power Law or Log Law for the Turbulent Boundary Layer?," *Bulletin of the American Physical Society*, Vol. 45, No. 9, 2000, p. 160.

[16] Gad-el-Hak, M., and Bandyopadhyay, P. R., "Reynolds Number Effects in Wall-Bounded Turbulent Flows," *Applied Mechanics Review*, Vol. 47, No. 8, 1994, pp. 307–365.

[17] Gill, A. E., "The Reynolds Number Similarity Argument," *Journal of Mathematical Physics*, Vol. 47, 1968, pp. 437–441.

[18] Österlund, J. M., Johansson, A. V., Nagib, H. M., and Hites, M. H., "A Note on the Overlap Region in Turbulent Boundary Layers," *Physics of Fluids*, Vol. 12, No. 1, 2000, pp. 1–4.

[19] Zanoun, E.-S., Nagib, H., Durst, F., and Monkewitz, P., "Higher Reynolds Number Channel Data and Their Comparison to Recent Asymptotic Theory," AIAA Paper 2002-1102, Jan. 2002.

[20] Spalart, P., "Direct Simulation of Turbulent Boundary Layer up to $Re_\theta = 1.410$," *Journal of Fluid Mechanics*, Vol. 187, Feb. 1989, pp. 61–98.

[21] Österlund, J. M., "Experimental Studies of Zero-Pressure Gradient Turbulent Boundary-Layer Flow," Ph.D. Dissertation, Dept. of Mechanics, Royal Inst. of Technology, Stockholm, Dec. 1999.

[22]Osaka, H., Kameda, T., and Mochizuki, S., "Re-examination of the Reynolds Number Effect on the Mean Flow Quantities in a Smooth Wall Turbulent Boundary Layer," *JSME International Journal, Series B*, Vol. 41, No. 1, 1998, pp. 123–129.

[23]Roach, P. E., and Brierley, D. H., "The Influence of a Turbulent Free Stream on Zero Pressure Gradient Transitional Boundary Layer Development. Part 1: Test Cases T3A and T3B," *Numerical Simulation of Unsteady Flows and Transition to Turbulence*, edited by D. Pironneau, W. Rode, and I. L. Ryhming, Cambridge Univ. Press, London, 1990.

[24]Gill, P. R., Murray, W., and Wright, M. H., "The Levenberg–Maquardt Method," *Practical Optimization*, Academic Press, London, 1981, Sec. 4.7.3, pp. 136, 137.

[25]Perry, A. E., Hafez, S., and Chong, M. S., "A Possible Reinterpretation of the Princeton Superpipe Data," *Journal of Fluid Mechanics*, Vol. 439, July 2001, pp. 395–401.

[26]Barenblatt, G. I., Chorin, A. J., and Prostokishin, V. M., "Self-Similar Intermediate Structures in Turbulent Boundary Layers at Large Reynolds Number," *Journal of Fluid Mechanics*, Vol. 410, May 2000, pp. 263–283.

[27]Barenblatt, G. I., Chorin, A. J., and Prostokishin, V. M., "Analysis of Experimental Investigations of Self-Similar Intermediate Structures in Zero-Pressure Boundary Layers at Large Reynolds Number," Center for Pure and Applied Mathematics, Univ. of California, Rept. PAM-777, Berkeley, CA, Jan. 2000.

[28]Coles, D., "The Law of the Wake in the Turbulent Boundary Layer," *Journal of Fluid Mechanics*, Vol. 1, Pt. 2, 1956, pp. 191–226.

[29]DeGraaff, D. B., and Eaton, J. K., "Reynolds-Number Scaling of the Flat Plate Turbulent Boundary Layer," *Journal of Fluid Mechanics*, Vol. 422, Nov. 2000, pp. 319–346.

P. Givi
Associate Editor

Color reproductions courtesy of the GE Fund and the Indiana 21th Century Research and Technology Fund.